











Ronin governs the metabolic capacity of the embryonic lineage for post-implantation development

Kirill Salewskij^{1,†} , Theresa Gross-Thebing^{1,†} , Elizabeth Ing-Simmons², Binyamin Duethorn¹, Bettina Rieger³, Rui Fan¹ , Rui Chen¹ , Niraimathi Govindasamy¹, Heike Brinkmann¹, Ludmila Kremer⁴, Nannette Kuempel-Rink⁴, Karina Mildner⁵ , Dagmar Zeuschner⁵ , Martin Stehling⁶, Marion Dejosez⁷, Thomas P Zwaka⁷, Hans R Schöler⁸ , Karin B Busch³ , Juan M Vaquerizas^{2,9,10}  & Ivan Bedzhov^{1,*} 

Abstract

During implantation, the murine embryo transitions from a “quiet” into an active metabolic/proliferative state, which kick-starts the growth and morphogenesis of the post-implantation conceptus. Such transition is also required for embryonic stem cells to be established from mouse blastocysts, but the factors regulating this process are poorly understood. Here, we show that Ronin plays a critical role in the process by enabling active energy production, and the loss of Ronin results in the establishment of a reversible quiescent state in which naïve pluripotency is promoted. In addition, Ronin fine-tunes the expression of genes that encode ribosomal proteins and is required for proper tissue-scale organisation of the pluripotent lineage during the transition from blastocyst to egg cylinder stage. Thus, Ronin function is essential for governing the metabolic capacity so that it can support the pluripotent lineage’s high-energy demands for cell proliferation and morphogenesis.

Keywords embryo; metabolism; implantation; Ronin; Thap11

Subject Categories Development; Metabolism; Stem Cells & Regenerative Medicine

DOI 10.15252/embr.202153048 | Received 12 April 2021 | Revised 23 August 2021 | Accepted 26 August 2021 | Published online 13 September 2021

EMBO Reports (2021) 22: e53048

Introduction

After fertilisation, the newly formed murine embryo undergoes several rounds of cleavage divisions in which progressively smaller cells (blastomeres) are generated while the total embryo volume stays constant. Cell fate decisions establish the first lineages, which self-organise by embryonic day four and a half (E4.5) into a hollow-shaped blastocyst. The blastocyst consists of a ball of naïve pluripotent cells (epiblast) surrounded by two extraembryonic tissues: the primitive endoderm (PE) and trophectoderm (TE). The TE mediates direct contact with the maternal tissues and initiates the implantation of the embryo into the uterine wall. Within 24 h, between E4.5 and E5.5, a burst of cell proliferation transforms the blastocyst into a post-implantation conceptus (egg cylinder) (Govindasamy *et al*, 2019). At the same time, the epiblast transforms from a simple ball of cells into a polarised epithelium (Bedzhov & Zernicka-Goetz, 2014; Fan *et al*, 2020), where during the next days the body axes are laid down and differentiation into somatic lineages is initiated.

The pluripotent properties of the epiblast are captured *in vitro* by embryonic stem cells (ESC), which are derived from blastocyst-stage embryos. Similar to the naïve epiblast, ESC express the core pluripotency transcription factors, namely Oct4 and Sox2, and a set of so-called “ancillary” transcription factors (e.g. Nanog, Esrrb, Klf4, Prdm14, Tbx3, Tfcp2l1 and Nr0b1). Altogether, the core and ancillary factors form a cross-regulated network, also known as the developmental or Oct4-centric module, which buffers against pro-

1 Embryonic Self-Organization Research Group, Max Planck Institute for Molecular Biomedicine, Münster, Germany

2 Regulatory Genomics Group, Max Planck Institute for Molecular Biomedicine, Münster, Germany

3 Institut für Integrative Zellbiologie und Physiologie, University of Münster, Münster, Germany

4 Transgenic Facility, Max Planck Institute for Molecular Biomedicine, Münster, Germany

5 Electron Microscopy Facility, Max Planck Institute for Molecular Biomedicine, Münster, Germany

6 Flow Cytometry Unit, Max Planck Institute for Molecular Biomedicine, Münster, Germany

7 Department for Cell, Regenerative and Developmental Biology, Black Family Stem Cell Institute, Icahn School of Medicine at Mount Sinai, Huffington Foundation Center for Cell-based Research in Parkinson’s Disease, New York, NY, USA

8 Department of Cell and Developmental Biology, Max Planck Institute for Molecular Biomedicine, Münster, Germany

9 MRC London Institute of Medical Sciences, London, UK

10 Institute of Clinical Sciences, Faculty of Medicine, Imperial College London, Hammersmith Hospital Campus, London, UK

*Corresponding author. Tel: +49 251 70365 370; E-mail: ivan.bedzhov@mpi-muenster.mpg.de

†These authors contributed equally to this work

differentiation cues and stabilises the undifferentiated ESC state (Dejosez & Zwaka, 2012; Hackett & Surani, 2014).

Other transcription factors, such as c-Myc, E2f1 and Ronin (Thap11), are involved in ESC proliferation and form the so-called cell growth module; these factors bind to promoters of genes involved in cell cycle regulation, metabolism and biosynthesis (Chen *et al.*, 2008; Dejosez *et al.*, 2010; Dejosez & Zwaka, 2012). The transcription factor Ronin belongs to a family of THAP (Thanatos-associated protein) domain-containing factors that originate from the P element transposon (Zwaka, 2008). Importantly, Ronin knockout (ko) embryos develop to blastocyst stage but then fail to form an egg cylinder, indicating that Ronin plays a critical yet not fully understood role for post-implantation embryogenesis (Dejosez *et al.*, 2008). Thus, we sought to understand why Ronin becomes indispensable upon implantation and what are the underlying cellular mechanisms that mediate this effect.

Results

Ronin depletion induces quiescent state in ESC

Ronin ko embryos form proper blastocysts that show no signs of cell death, but, somewhat unexpectedly, ESC cannot be directly established from these embryos (Dejosez *et al.*, 2008; Zwaka, 2008). To bypass this limitation and first analyse the effects of Ronin depletion *in vitro*, we used a conditional ko ESC line, where one of the Ronin alleles is deleted and the second is flanked by loxP sites (floxed) (Dejosez *et al.*, 2008; Seifert *et al.*, 2017). These cells express Cre-ERT2 recombinase (Ronin fl/del Cre-ERT2), which enables the inducible excision of the Ronin coding sequence upon treatment with 4-hydroxytamoxifen (4OHT). Thus, to delete Ronin, we supplemented the ESC culture medium with 4OHT and analysed the timing of Ronin depletion. We found that compared to in control non-treated cells, in treated cells Ronin becomes undetectable on the protein level within 2 days of culture (Figs 1A and EV1A).

Next, we examined the proliferation, apoptosis and expression of key pluripotency markers in Ronin ko ESC. Both control (Ronin fl/del) and Ronin ko (Ronin del/del) cells established typical dome-shaped colonies and were indistinguishable up to days 4–5 of culture. After that, the ko cells exhibited a substantially reduced growth rate (Fig 1B and C), which was not associated with an increase in cell death, determined by Annexin V staining (Fig 1D). Moreover, the cell cycle distribution was similar between control and ko cells, indicating that Ronin ko ESC do not exhibit a block in a particular phase of the cell cycle (Fig 1E and F). At day 4 and day 8 of culture, Ronin ko ESC

expressed the pluripotency factors Oct4, Sox2 and Nanog and displayed no signs of differentiation (Figs 1G and EV1B–D). Thus, Ronin ko ESC gradually decrease their proliferation rate, without losing expression of the core pluripotency transcription factor circuit.

The quiescent state in Ronin-deficient ESC is reversible

To understand whether the quiescent state in Ronin ko ESC is reversible, we generated an ESC line where Ronin expression can be dynamically modulated. We stably transfected Ronin fl/del Cre-ERT2 cells with a doxycycline (Dox)-inducible FLAG-tagged Ronin construct. After 4OHT treatment, the conditional allele in these cells was deleted, generating a del/del background. Thus, upon Dox stimulation, only the expression of the ectopic Ronin-FLAG construct (ecto-Ronin) was detectable (Fig 2A). Using this system, we examined whether Ronin ko cells can be rescued and reverted back to a proliferative state. As expected, in the absence of Dox the cells exhibited a lower growth rate compared to ESC continuously grown in Dox-supplemented medium. However, a subsequent Dox stimulation boosted the cell proliferation of the ecto-Ronin cells to a similar level as the uninterrupted +Dox control (Fig 2B). Moreover, the “rescued” cells formed teratomas upon subcutaneous injection in mice on a diet of Dox-containing food (Fig 2C and D). The solid tumours comprised derivatives of all three germ layers, indicating proper differentiation potential of the donor ESC. In contrast, Ronin del/del ESC failed to give rise to teratomas, precluding further multi-lineage differentiation analysis (Fig 2C–E).

To test whether Ronin ko ESC have at least some potential for early lineage differentiation, we generated embryoid bodies (EBs) and analysed the expression of anterior (Sox2) and posterior—mesodermal (Vimentin) and definitive endoderm (Gata6 and Sox17) marker genes. We found that Ronin ko ESC can give rise to cell populations positive for anterior and mesodermal markers. However, in contrast to control Ronin fl/del and Dox-treated ecto-Ronin cells, Ronin ko EBs did not show any expression of definitive endoderm genes (Fig 2F). This indicates that Ronin ko ESC can exit the naïve pluripotent state and initiate somatic differentiation, and the lack of definitive endoderm makers may be an indirect effect of the slow growth rate; nonetheless, we cannot exclude that Ronin may play a yet unknown role in the specification or maintenance of the endoderm lineage.

Long-term depletion of Ronin reinforces the naïve pluripotency network

Next, we performed RNA-seq analysis to examine the transcriptional response to Ronin depletion in day 4 and day 8 ko ESC (Fig 3A).

Figure 1. Ronin depletion induces quiescent state in ESC.

- A Western blot analysis of Ronin depletion upon treatment of Ronin fl/del Cre-ERT2 cells with 4OHT.
- B Brightfield images of Ronin fl/del and Ronin del/del ESC.
- C Cell count of Ronin fl/del and Ronin del/del ESC. Data represent mean \pm SD, $n =$ three independent experiments.
- D Annexin V cell death assay of Ronin fl/del and Ronin del/del cultured for 6 days. Two-tailed unpaired Student's t test, data represent mean \pm SD, $n =$ three independent experiments.
- E FACS plot of cell cycle distribution of day 6 Ronin del/del and Ronin fl/del, determined by EdU assay.
- F Quantification of the cell cycle distribution determined by EdU assay. Data represent mean \pm SD, $n =$ three independent experiments.
- G Ronin fl/del and Ronin del/del ESC stained for Ronin (left panel) or Oct4 (right panel). The nuclei are counterstained with DAPI.

Data information: Scale bars (B), 100 μ m; (G), 10 μ m. See also Fig EV1.
Source data are available online for this figure.

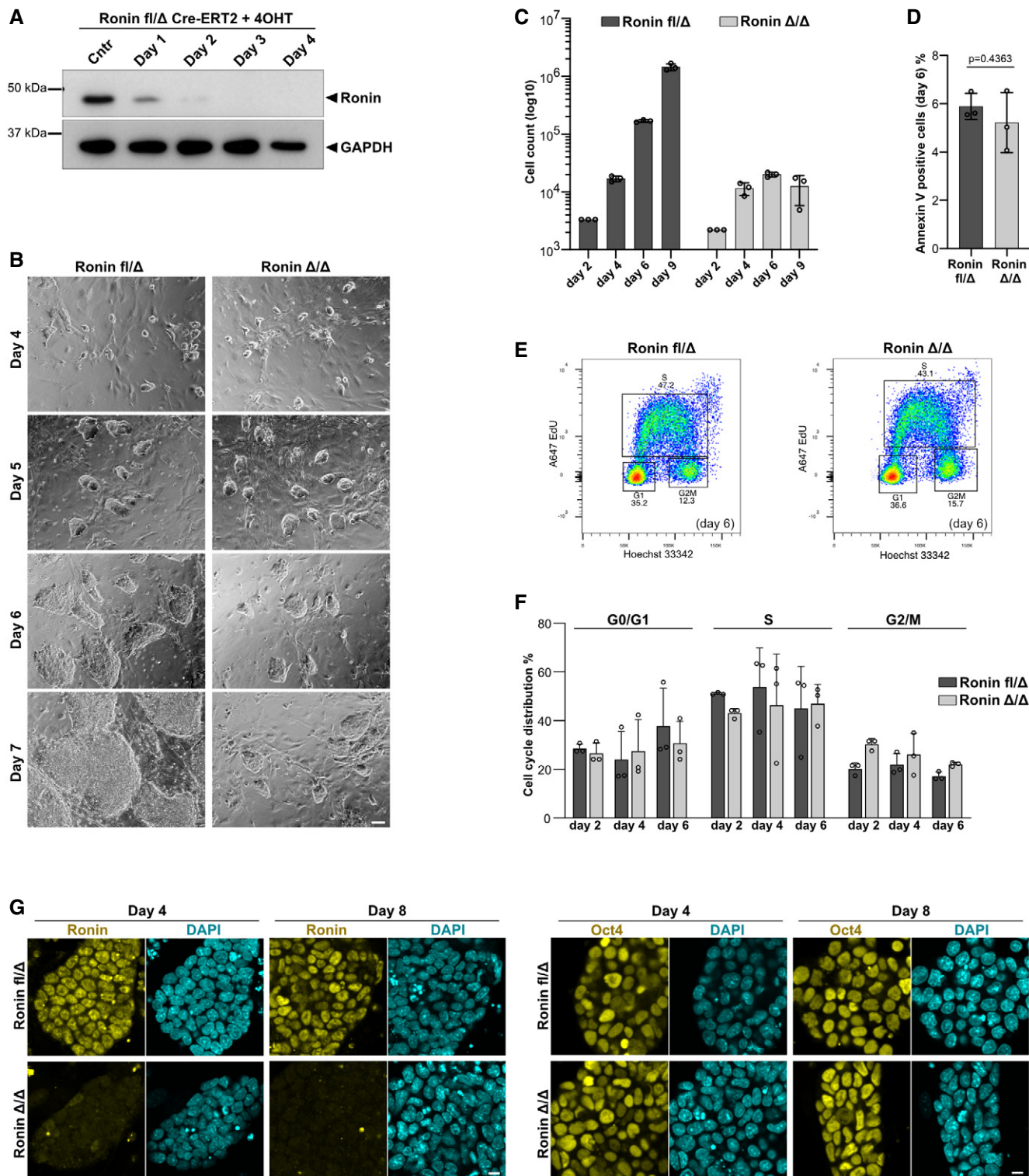


Figure 1.

First, we analysed the expression of pluripotency factors and found gradual upregulation of naïve markers such as Tfcp2l1, Nanog and Prdm14. At the same time, markers associated with exiting naïve pluripotency and entering into a primed state, such as Dmmt3b, Dmmt3a and Otx2, were downregulated (Fig 3B and C).

Tfcp2l1 was the most highly upregulated pluripotency factor in Ronin ko ESC at culture day 8 (Fig 3B). Tfcp2l1 is a major transcription factor that promotes pluripotency downstream of the Lif/Stat3 pathway and is also required for ESC responsiveness to Lif stimulation (Martello *et al*, 2013; Ye *et al*, 2013). Several other Lif/Stat3

target genes such as *Gbx2*, *Klf4* and *Tcl1* were also upregulated. Accordingly, gene set enrichment analysis (GSEA) revealed that Ronin ko ESC had an increased expression of *Il6/Jak/Stat3* signalling components (Figs 3D and EV2A). For instance, *Il6*, *Lif* receptor (*LifR*) and *Cd9* tetraspanin, which stabilises the *Il6* receptor (*gp130*) on the cell membrane (Shi *et al*, 2017), were upregulated in Ronin-deficient ESC. To examine whether Ronin directly binds to the promoters of these factors, we analysed available Ronin ChIP-seq

data (Hnisz *et al*, 2013) and found no enrichment on *Il6/Lif* signalling-related genes (Figs 3E and EV2A). Similarly, Ronin did not directly bind the promoters of the examined core, naïve or primed pluripotency factors (Fig 3C), in agreement with previous reports (Dejosez *et al*, 2008, 2010). Altogether, this shows that Ronin does not directly reinforce the naïve pluripotency network; instead, the reinforcement is a gradual response that builds up as the cells' proliferation rate decreases.

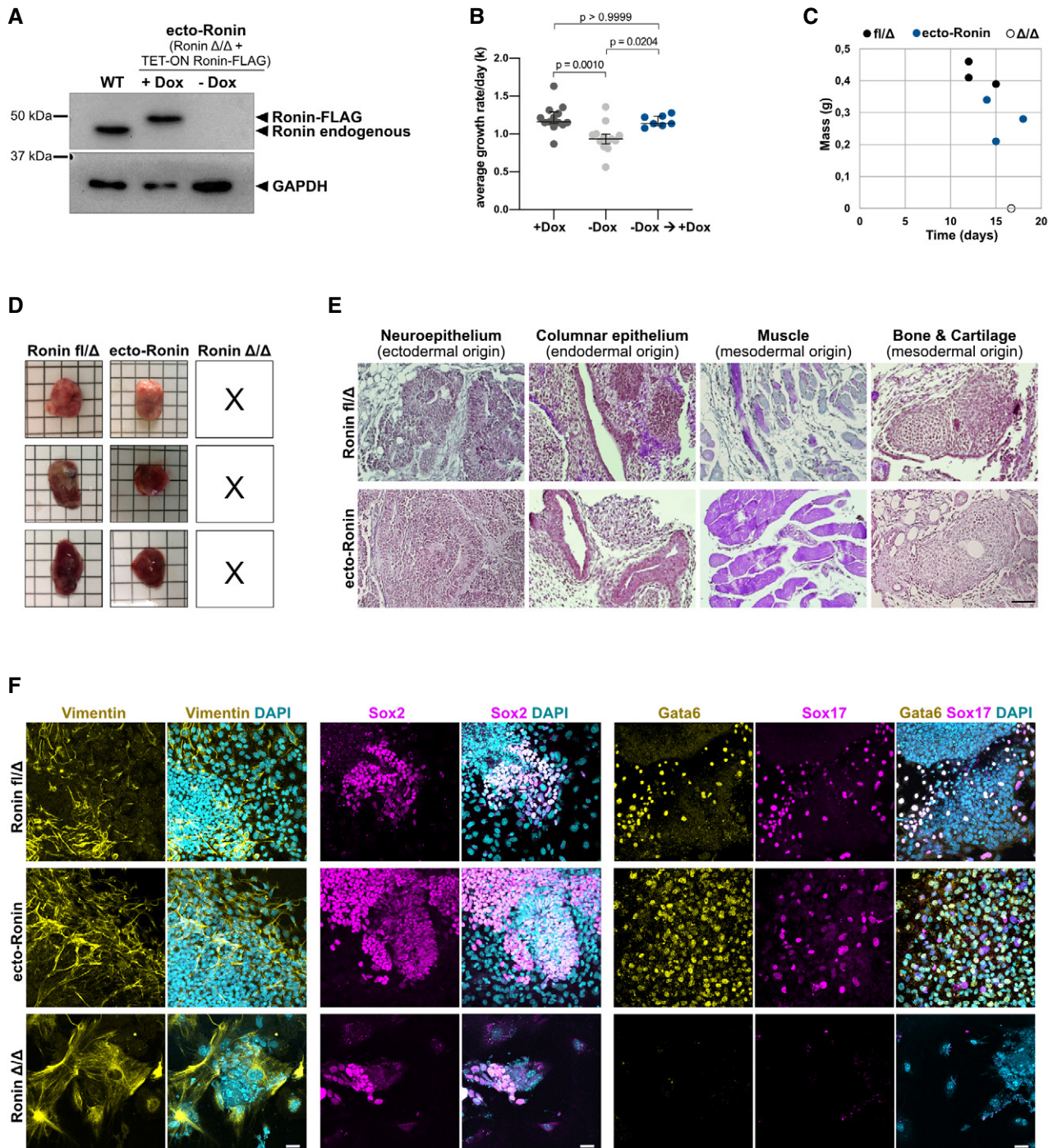


Figure 2.

Figure 2. The quiescent state in Ronin-deficient ESC is reversible.

- A Western blot analysis of ecto-Ronin expression Ronin del/del + TET-ON Ronin-FLAG ESC cultured in the presence of Dox or without Dox for 3 days. The endogenous levels of Ronin are compared to wild-type (WT) E14 ESC.
- B Average growth rate per day (k) of ecto-Ronin (Ronin del/del TET-ON Ronin-FLAG) ESC cultured continuously in the presence of Dox (+Dox); without Dox for 5 passages (-Dox) or grown without Dox for 3 passages and then switched to Dox-containing medium for another 2 passages (-Dox → +Dox). Ordinary one-way ANOVA, error bars represent median with interquartile range, technical replicates (+Dox, $n = 13$), (-Dox $n = 13$), (-Dox → +Dox, $n = 7$) of three independent experiments.
- C Tumour growth of Ronin fl/del, ecto-Ronin and Ronin del/del teratomas, n teratomas for each genotype = 3.
- D Brightfield images of teratomas derived from Ronin fl/del and ecto-Ronin ESC.
- E Haematoxylin/eosin staining of paraffin sections of Ronin fl/del and ecto-Ronin teratomas.
- F *In vitro* differentiation of Ronin fl/del, ecto-Ronin (grown in the presence of Dox) and Ronin del/del ESC.
- Data information: Scale bars (E), 50 μm ; (F), 40 μm .
Source data are available online for this figure.

To gain insight into the underlying mechanism that induces a quiescent state in Ronin ko ESC, we applied whole transcriptome hierarchical clustering and delineated the globally upregulated (clusters 1 and 2) and downregulated (clusters 3, 4 and 5) sets of genes (Figs 3F and EV2B). Using these defined clusters, we performed a gene ontology (GO) analysis to generally understand the associated cellular and molecular functions of each subgroup. In clusters 1 and 2, the main GO terms included epithelial migration, adherens junction and extracellular matrix; cluster 3 was associated with GO terms such as Rab GTP-ase binding and Rab-GEF activity (Figs 3G and EV2C). Thus, clusters 1, 2 and 3 contained genes that are related to epithelial morphology and intracellular trafficking, indicating that loss of Ronin function may affect the tissue-scale organisation of the pluripotent cells.

The genes grouped in clusters 4 and 5 were associated with several ribosomal GO terms, such as cytosolic ribosome, preribosome and ribonucleoprotein complex assembly. As protein synthesis is integral for cell homeostasis and proliferation, in the following experiments we took a closer look at the expression of genes encoding ribosomal factors and examined the net effect of Ronin depletion on the process of translation.

Loss of Ronin tunes down the expression of genes encoding ribosomal proteins

First, we compared the gene expression of day 8 vs. day 4 Ronin ko ESC and found that an array of genes encoding ribosomal proteins, such as Rpl4, Rpl21 and Rpsa, exhibited reduced expression at day 8 (Fig 4A). Accordingly, GO analysis of the downregulated genes (day 8 vs. day 4) revealed GO terms associated with ribosomal structure and biogenesis (Fig 4B). Thus, we examined the expression of all genes encoding cytoplasmic ribosomal proteins and found consistent, global downregulation in Ronin ko ESC (Fig 4C).

Moreover, ChIP-seq analysis revealed that Ronin binds to the promoters of several ribosomal factors, such as Rpl18a, Rpl7, Rpl15 and Rpl2, indicating that these factors are potential direct downstream targets (Fig 4C and D).

To generally understand the cellular function of the genes directly bound by Ronin, we applied GO enrichment analysis to the ChIP-seq dataset. In addition to the GO terms ribonucleoprotein complex biogenesis and structural constituent of ribosomes, another top GO term was mitochondrial protein complex (Fig 4E). Therefore, we examined the expression of all genes encoding mitochondrial ribosomal proteins and found overall downregulation of these factors in Ronin ko ESC (Fig EV3A and B).

To understand the extent to which the downregulation of genes encoding ribosomal proteins affects the protein biosynthesis in Ronin ko ESC, we performed an OP-puro (O-propargyl-puromycin) assay. OP-puro integrates into nascent polypeptide chains, and after that, the incorporated OP-puro is detected via a click-chemistry reaction with fluorescently tagged azide (Liu *et al*, 2012). Using this assay, we analysed the nascent protein production in control (Ronin fl/del), Dox-treated ecto-Ronin and Ronin ko (day 4 and day 8) cells. We found no significant decrease in the OP-puro signal in Ronin-deficient cells compared to control ESC (Fig 4F and G). Thus, although the loss of Ronin tunes down the expression of genes encoding ribosomal proteins, the net effect of Ronin loss on the protein biosynthesis cannot account for the decelerated proliferation of Ronin ko ESC.

Ronin function is required for proper mitochondrial cristae formation and function

The ChIP-seq GO analysis also revealed that Ronin directly binds to genes involved in the structure of the mitochondria and the organisation of the inner mitochondrial membrane (Fig 4E). The inner

Figure 3. Transcriptional analysis of Ronin ko ESC.

- A Principal component analysis (PCA) of Ronin fl/del, Ronin del/del (day 4) and Ronin del/del (day 8) transcriptomes; $n = 3$ independent RNA-seq datasets for each condition.
- B Volcano plot of gene expression in Ronin del/del day 4 vs. Ronin fl/del (left panel) and Ronin del/del day 8 vs. Ronin fl/del ESC (right panel) with annotated naïve and primed pluripotency markers.
- C Expression and binding of Ronin to core, naïve and primed pluripotency markers.
- D Gene set enrichment analysis (GSEA) plot of Il6/Jak/Stat3 signalling, day 8 Ronin ko ESC.
- E Expression and binding of Ronin to Il6/Lif signalling-related genes.
- F K-means clustering of 5 major groups of genes in Ronin fl/del, Ronin del/del (day 4) and Ronin del/del (day 8) transcriptomes.
- G Gene ontology (GO) enrichment analysis of the predefined gene clusters—molecular function (left panel) and cellular component (right panel). See also Fig EV2.

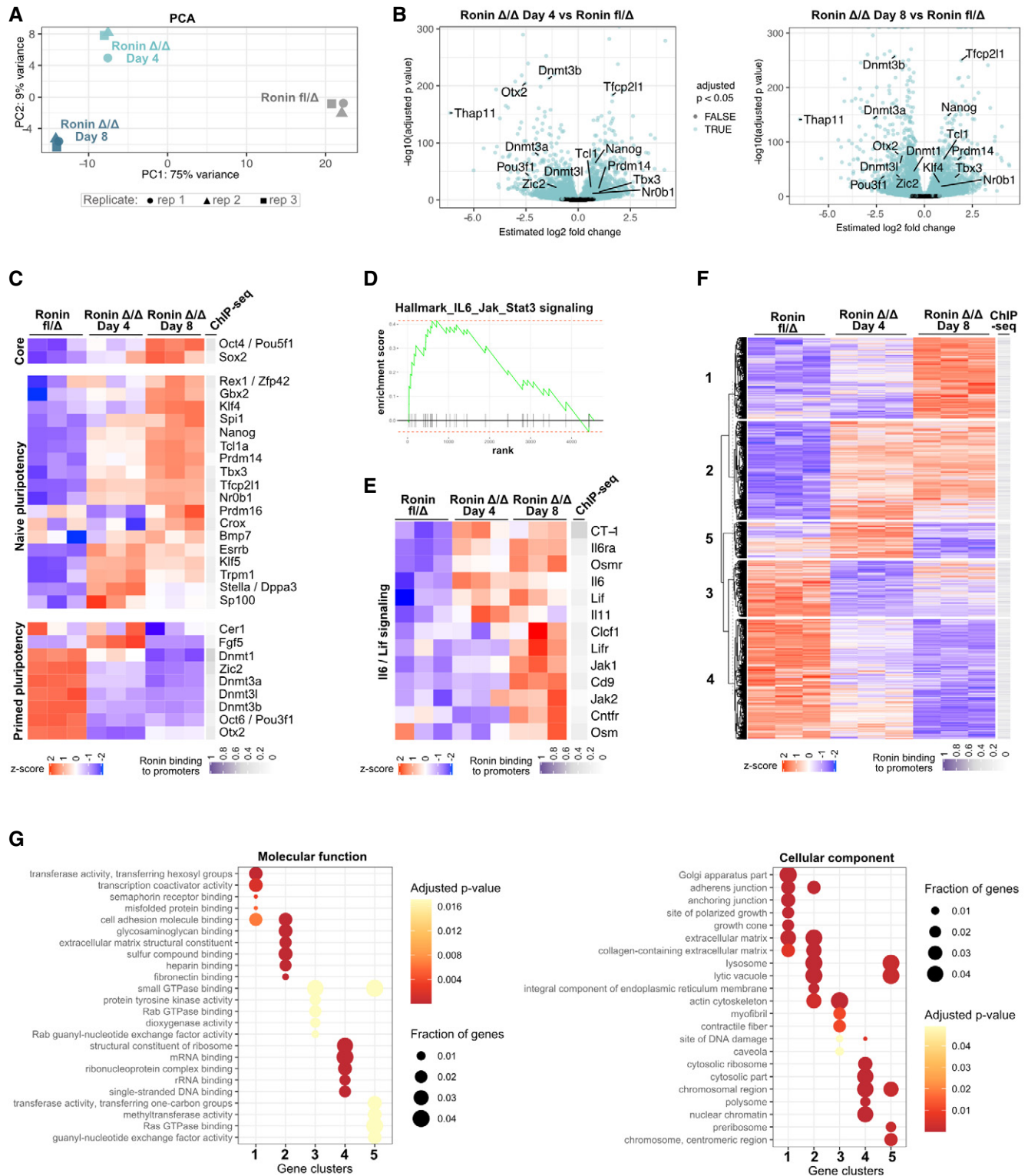


Figure 3.

membrane forms invaginations (cristae), increasing its surface area, and hosts the electron transport chain (ETC) and ATP synthase, which generate adenosine triphosphate (ATP) via oxidative phosphorylation (Mishra & Chan, 2014). We found that Ronin binding is

enriched on promoters of genes encoding critical structural proteins of the inner membrane such as *Opa1* and *Letm1* (Tamai *et al.*, 2008; Mishra & Chan, 2014) as well as factors regulating cristae formation, such as *Tmem11* and *Adck1* (Rival *et al.*, 2011) (Fig 5A and B).

Figure 4. Ronin tunes the expression of genes encoding ribosomal proteins.

- A Volcano plot of gene expression in Ronin del/del day 8 vs. Ronin del/del day 4 ESC.
 B GO enrichment analysis of Ronin del/del day 8 vs. Ronin del/del day 4 downregulated genes. BP, biological process; CC, cellular component; MF, molecular function.
 C Expression and binding of Ronin to genes encoding cytoplasmic ribosomal proteins.
 D Binding of Ronin to the promoters of genes encoding cytoplasmic ribosomal proteins.
 E GO enrichment analysis of genes that are directly bound by Ronin. BP, biological process; CC, cellular component; MF, molecular function.
 F Analysis of nascent protein synthesis using OP-puro assay. Ronin fl/del cells treated with protein synthesis inhibitor (cycloheximide) are used as negative control. The nuclei are counterstained with DAPI.
 G Quantification of the OP-puro signal, normalised to DAPI. Ordinary one-way ANOVA data represent mean \pm SD; $n =$ three independent experiments for each genotype.
 Data information: Scale bar (F), 15 μ m. See also Fig EV3.

Moreover, Ronin depletion resulted in the downregulation of these factors (Fig 5A), which can lead to structural changes in the mitochondria, alterations in the function of the ETC and a reduction in energy production.

To test this hypothesis, first we performed ultrastructural analysis of the mitochondria in control and Ronin ko ESC using transmission electron microscopy. We found a gradual loss of cristae in day 4 and day 8 Ronin ko ESC (Fig 5C), resembling the previously described effects of Letm1 or Adck1 knock down in HeLa cells (Tamai *et al*, 2008; Yoon *et al*, 2019).

Next, we analysed the mitochondrial transmembrane potential ($\Delta\Psi_m$) using the tetramethyl-rhodamine ethyl ester (TMRE) assay, which provides information about the general health status of mitochondria (Crowley *et al*, 2016). We found that the TMRE signal intensity was reduced in Ronin ko cells (Fig 5D and E). As the energy required for ATP production is derived from the $\Delta\Psi_m$ (Mitchell, 1961), this suggests that Ronin ko cells exhibit a decreased energy availability for ATP synthesis.

To examine the oxygen consumption rate (OCR), we used an automatic flux analyser (Seahorse/Agilent) and conducted a mitochondrial stress test assay. This assay measures the OCR before and after applying inhibitors of different ETC components, thereby providing an assessment of multiple mitochondrial respiration parameters. We found that the proton leak, which indicates the remaining respiration not coupled to ATP synthesis, was reduced in Ronin-deficient cells (Fig 5F and G). In addition, we found that the basal and maximal respiration, as well as the ATP-linked respiration and the non-mitochondrial oxygen consumption, were substantially decreased in Ronin ko ESC (Fig 5F and G). Taken together, the reduced level of all measured parameters indicates that the loss of cristae in Ronin ko ESC globally affects the ETC complexes, resulting in a general reduction of the mitochondrial ATP production rate and energy efficiency.

Ronin governs metabolic competency of post-implantation growth and morphogenesis

Next, we examined the expression of Ronin and the structure of the mitochondria in blastocyst- and egg cylinder-stage embryos. We also analysed diapause blastocysts, as diapause embryos reside in a natural, *in vivo* state of metabolic dormancy (Fenelon *et al*, 2014; Fan *et al*, 2020). We found nuclear expression of Ronin in all of the examined developmental stages (Fig 6A). In addition, we analysed an available RNA-seq dataset of the pluripotent lineage in E4.5, diapause and E5.5 embryos (Boroviak *et al*, 2015) and found that Ronin is transcriptionally upregulated in the post-implantation epiblast (Fig EV4).

The ultrastructural analysis revealed that the post-implantation epiblast contains elongated mitochondria with well-established cristae (Fig 6B). The morphology of the E5.5 mitochondria indicates progressive maturation, which coincides with the greater amount of energy required for supporting the extensive cell proliferation of the post-implantation epiblast. In contrast, the mitochondria in the pluripotent lineage of the E4.5 and dormant blastocysts were smaller, round and had a low density of cristae, in line with previous reports (Fu *et al*, 2014; Lima *et al*, 2018) (Fig 6B). As embryo growth and mitochondrial maturation kick-start after implantation, this suggests that Ronin deficiency can be tolerated up to the blastocyst stage and potentially during diapause. However, Ronin function is supposedly indispensable for proper post-implantation development and most likely for reactivating embryo growth upon exiting diapause.

To test this hypothesis, we carried out a set of experiments examining the role of Ronin *in vivo*. As Ronin ko embryos do not develop beyond the blastocyst stage (Dejosez *et al*, 2008), we generated embryo / ESC chimeras. This approach allowed us to analyse Ronin loss of function in the context of the epiblast and, at the same time,

Figure 5. Ronin controls mitochondrial cristae formation and function.

- A Expression and binding of Ronin to structural and regulatory factors of the mitochondrial cristae.
 B Binding of Ronin to the promoters of mitochondrial cristae genes.
 C Transmission electron microscopy analysis of mitochondrial structure in Ronin fl/del and Ronin del/del ESC. Mitochondria analysed, $n > 150$ for each condition.
 D Flow cytometry analysis of Ronin fl/del and Ronin del/del stained for MitoTracker and TMRE.
 E Quantification of the TMRE signal determined by the flow cytometry analysis. Ordinary one-way ANOVA, data represent mean \pm SEM, $n =$ three independent experiments.
 F OCR measurement using the Seahorse mitochondrial stress test assay. FCCP, Carbonyl cyanide-4 (trifluoromethoxy) phenylhydrazone; Rot, Rotenone; AA, Antimycin, data represent the mean of 2 independent experiments.
 G Quantification of the OCR analysis. Kruskal–Wallis test, bar graphs represent the mean, $n = 16$ technical replicates per genotype from 2 independent experiments.
 Data information: Scale bars (C), 1 μ m.

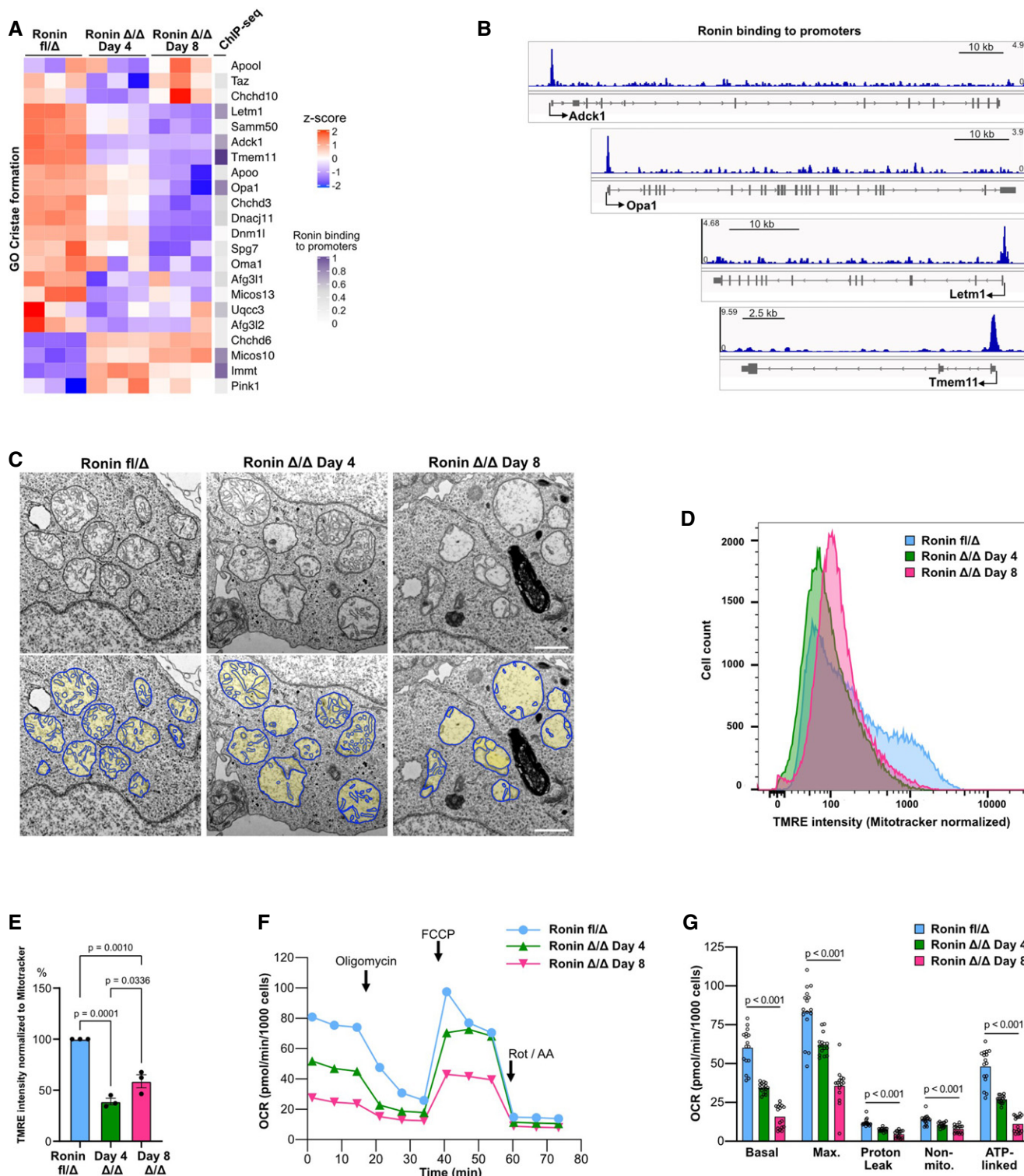


Figure 5.

enabled post-implantation embryogenesis. We incorporated fluorescently labelled Ronin ko ESC at day 4 or control (Ronin fl/del) ESC into 8-cell stage morulae (Fig 7A). At the late blastocyst stage, we quantified the number of donor cells, marked by Histone-H2B:

tdTomato expression, and found no substantial difference between the two groups (Fig 7C and D).

To test whether Ronin ko cells can be maintained in the epiblast during embryo dormancy, we transferred the chimeric blastocysts

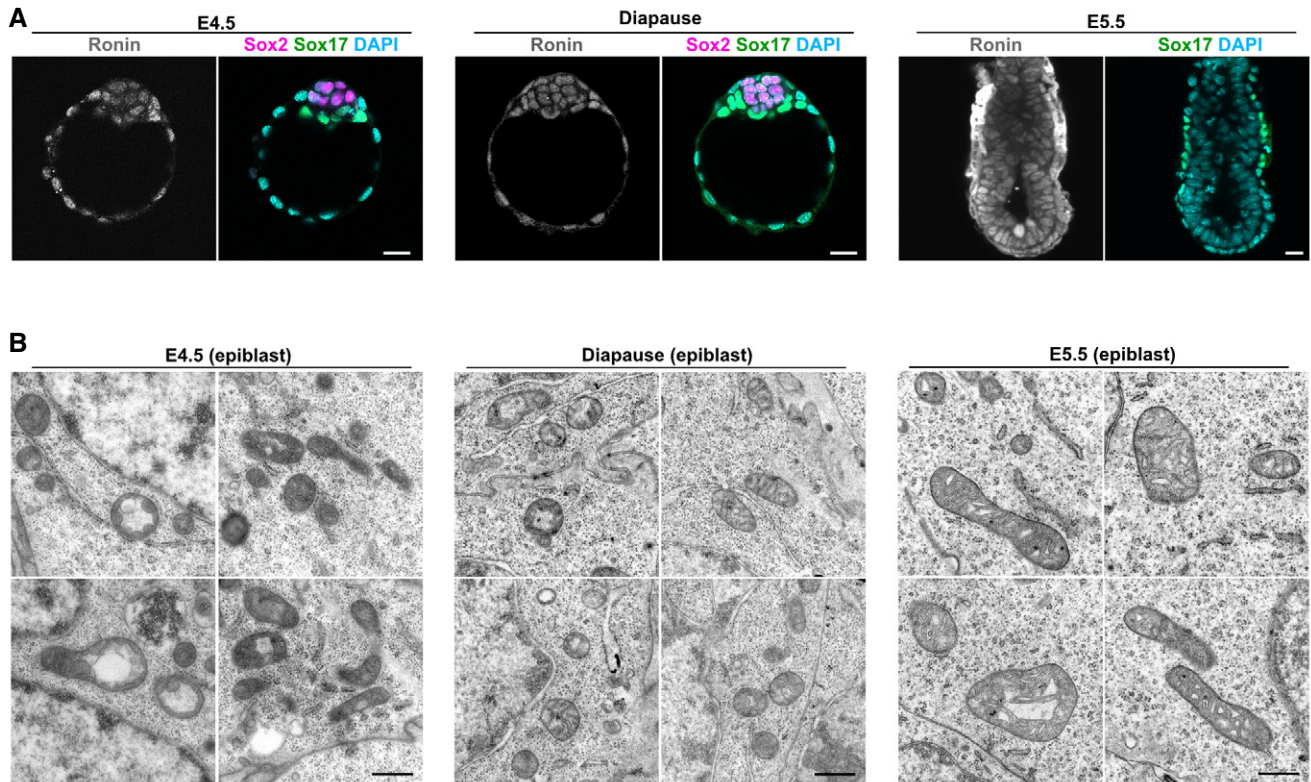


Figure 6. Expression of Ronin and mitochondrial morphology in early embryos.

A Blastocyst (E4.5) and diapause embryos stained for Ronin, Sox2 and Sox17. Egg cylinder-stage (E5.5) embryo stained for Ronin and Sox17. Nuclei are counterstained with DAPI.

B Transmission electron microscopy analysis of mitochondrial morphology in the epiblast of E4.5, diapause and E5.5 embryo. Mitochondria analysed, E4.5 (n mitochondria = 55), diapause (n mitochondria = 62), E5.5 (n mitochondria = 65).

Data information: Scale bar (A), 20 μ m; (B), 500 μ m. See also Fig EV4.

Figure 7. Ronin function is essential for the post-implantation growth and morphogenesis of the embryonic lineage.

A Schematic representation of the generation of chimeric embryos.

B Schematic representation of the induction of diapause and reactivation of chimeric embryos.

C E4.5 chimeric embryos stained for tdTomato and DAPI.

D Quantification of donor cells' contribution in E4.5 blastocysts, Mann–Whitney test, data represent mean \pm SD; Ronin fl/del n embryos = 26, Ronin del/del n embryos = 27.

E Diapause embryos stained for tdTomato and DAPI.

F Quantification of donor cells' contribution in diapause embryos, unpaired Student's t test, data represent mean \pm SD, Ronin fl/del n embryos = 4, Ronin del/del n embryos = 12.

G E5.5 chimeric embryos stained for tdTomato and DAPI.

H Quantification of donor cells' contribution in E5.5 embryos, unpaired Student's t test, data represent mean \pm SD, Ronin fl/del n embryos = 21, Ronin del/del n embryos = 15.

I Reactivated E5.5 chimeric embryos stained for tdTomato and DAPI.

J Quantification of donor cells' contribution in reactivated E5.5 embryos, Mann–Whitney test, data represent mean \pm SD, Ronin fl/del n embryos = 17, Ronin del/del n embryos = 12.

K E7.5 chimeric embryos stained for tdTomato and DAPI.

L Quantification of donor cells' contribution in E7.5 embryos, data represent mean \pm SD, Ronin fl/del n embryos = 14, Ronin del/del n embryos = 8.

M E5.5 chimeric embryos stained for Podocalyxin, tdTomato, E-cad and DAPI.

N Ronin fl/del and Ronin del/del (day 4) cells grown in 3D culture conditions for 48 h and stained for apical polarity markers – Podocalyxin and Par6, as well as Phalloidin, E-cad and tdTomato.

O Quantification of Par6-positive and Par6-negative ESC clumps of Ronin fl/del (n = 44) and Ronin del/del (n = 13) cells grown in 3D culture conditions for 48 h.

Data information: Scale bars, (C), (E), (G), (I), 25 μ m; (K), 100 μ m; (M), 20 μ m; (N), 10 μ m.

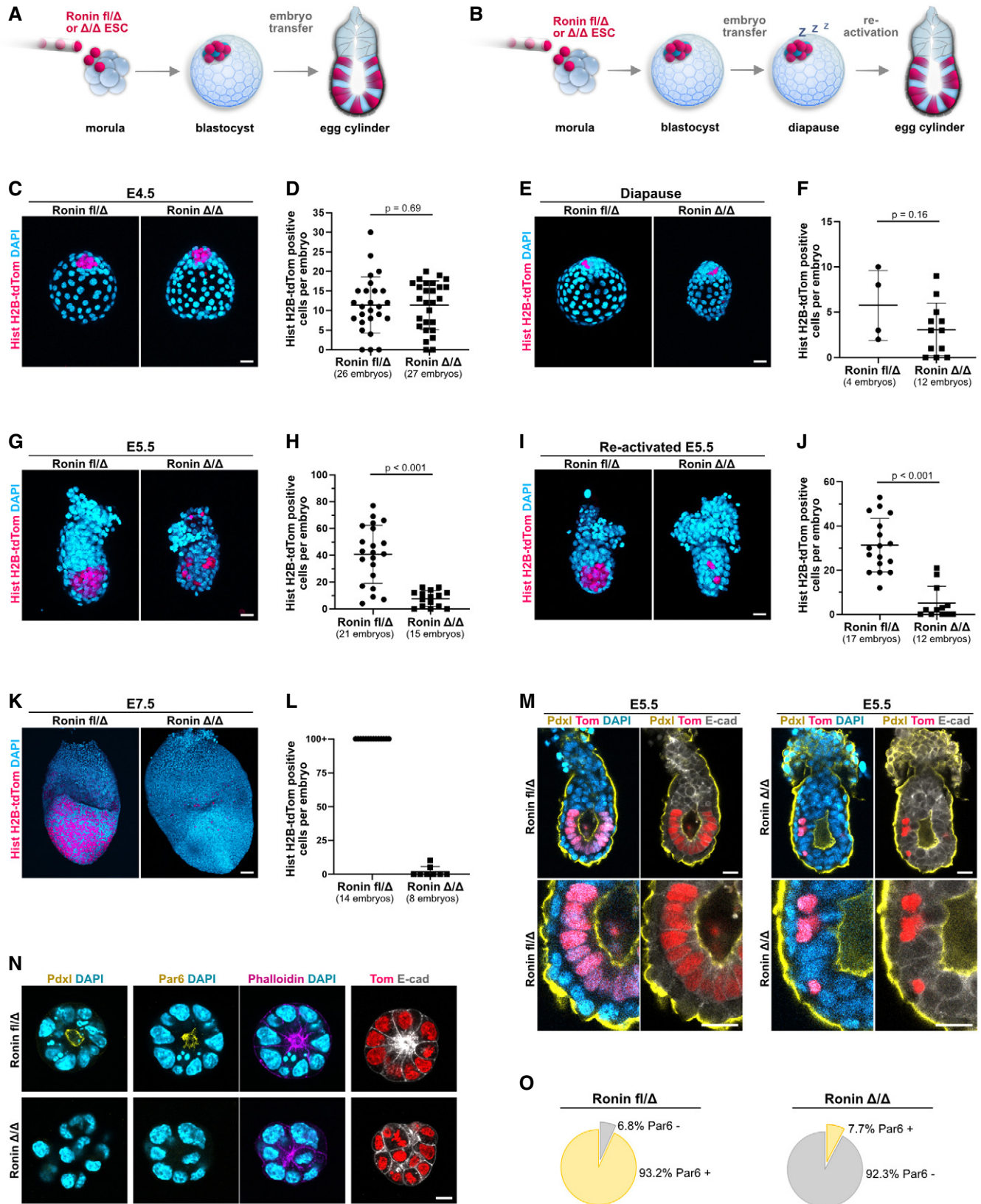


Figure 7.

into foster mothers and induced diapause via ovariectomy (Fig 7B). Again, we found a similar number of both Ronin ko and control donor cells in the dormant epiblast (Fig 7E and F).

Next, we examined the contribution of Ronin ko cells to the post-implantation epiblast. We found that at E5.5 and later at E7.5, the control Ronin fl/del cells progressively expanded, whereas the proliferation of Ronin ko cells was severely impeded (Fig 7G and H, and K and L). Similarly, upon exit of diapause the control cells exhibited rapid proliferation in the reactivated embryos, whereas Ronin ko cells appeared quiescent (Fig 7I and J). Altogether, this indicates that Ronin plays a critical role in the growth of the post-implantation epiblast as well as for the re-entry of the pluripotent lineage into the proliferative state upon exiting embryo dormancy.

Finally, we analysed the organisation of the Ronin ko cells in the context of the post-implantation epiblast. The control Ronin fl/del cells formed polarised pseudostratified epithelium, surrounding the central proamniotic cavity, whereas the Ronin ko cells failed to establish epithelial polarity (Fig 7M). To independently validate these observations, we used a previously established 3D culture model of epiblast morphogenesis, where ESC grown into a hydrogel of extracellular matrix proteins (matrigel) undergo de novo epithelialisation and lumenogenesis *in vitro* (Bedzhov & Zernicka-Goetz, 2014; Fan *et al*, 2020). We found that control cells grown in 3D culture conditions efficiently established a Podocalyxin/Par6-positive apical domain and central lumen, whereas Ronin ko cells remained unorganised (Fig 7N and O). Thus, Ronin ko cells exhibited impaired morphogenesis, which could be the net effect of having an inadequate energy supply for tissue remodelling and potential dysregulation of epithelial factors, as suggested by the RNA-seq data.

Taken together, these analyses show that embryos depend on Ronin function at the time of mitochondrial maturation, during the accelerated growth of the post-implantation epiblast. Thus, Ronin is dispensable for the development of the pluripotent lineage during the pre-implantation embryogenesis, but it is critical for providing enough metabolic capacity for the post-implantation epiblast, which has high-energy demands for cell proliferation and morphogenesis.

Discussion

During the development from the zygote to the blastocyst stage, progressively smaller blastomeres are generated via cleavage divisions, while the total amount of mitochondria in the embryo remain constant. Thus, the number of mitochondria per cell halves with each division (Cree *et al*, 2008). In addition to the continuous reduction in number, the mitochondria in the pre-implantation embryo are immature, resulting in low oxygen consumption and reduced ATP production (Quinn & Wales, 1971; Lima *et al*, 2018); thus, the cleavage embryos are referred as metabolically “quiet” (Leese, 2012). The metabolic rate further slows down and the embryos become quiescent during diapause (Fenelon *et al*, 2014; Fu *et al*, 2014), a reversible state of biosynthetic/metabolic dormancy that is induced as an adaptive response to environmental factors via suppression of oestrogen production. During diapause, development arrests at the blastocyst stage, but any time there is a peak of oestrogen, including exogenously provided, embryogenesis can be reactivated, triggering an exit from dormancy and the initiation of implantation (Fenelon *et al*, 2014; Fan *et al*, 2020).

During implantation, the blastocyst adheres and invades the uterine wall, establishing the first direct contact with the mother. In turn, the maternal tissues engulf the embryo, which quickly transforms into a post-implantation conceptus (egg cylinder). This transition is mediated by a burst of cell proliferation and extensive reorganisation in the tissue architecture of the developing embryo (Govindasamy *et al*, 2019). The gradual acceleration of cell proliferation after implantation has been first described by M. Snow, who examined histologically the cells numbers in the murine embryos between E4.5 and E7.5 (Snow, 1977). Accordingly, our ultrastructural analysis of the E5.5 epiblast revealed progressive mitochondrial maturation, coinciding with the initiation of embryo growth. Although the low cell number precludes lineage-specific analysis of metabolic signatures *in vivo*, the mitochondrial maturation in the post-implantation epiblast is most likely necessary to boost the ATP production in order to meet the energy demand of cell proliferation. Moreover, it is plausible that an adequate energy supply is also required to fuel cellular processes that mediate the morphogenesis of the pluripotent lineage, such as ion pump activity, vesicle transport and the synthesis of new building blocks.

Although ESC are derived from the epiblast of “quiet” pre-implantation embryos, they display rapid proliferation, generating biomass in a form of dome-shaped colonies. This *in vitro* adaptation essentially enables the establishment of ESC lines, which can self-renew potentially indefinitely. In contrast to the pre-implantation epiblasts, ESC are metabolically active and exhibit high oxygen consumption through mitochondrial respiration (Houghton, 2006; Zhang *et al*, 2018). This suggests that a transition from a “quiet” to an active metabolic/proliferative state is a prerequisite for ESC lines derivation from blastocyst-stage embryos (Fig 8). It is plausible that the absence of Ronin hinders this transition, which would explain why it is not possible to establish ESC from Ronin ko embryos. In line with this notion, we found that conditional deletion of Ronin in ESC results in a gradual loss of cristae, reduced mitochondrial respiration and entry into a quiescent state.

In vivo, Ronin function becomes indispensable only when the pluripotent lineage enters into an active metabolic/proliferative state following implantation. Ronin ko cells appeared quiescent in the context of the post-implantation embryo and also failed to establish proper polarised epithelium at E5.5. This indicates that Ronin is essential for governing the adequate metabolic capacity needed to support the cell proliferation and morphogenesis of the post-implantation epiblast (Fig 8). The impaired morphogenesis of Ronin ko cells could be a pleiotropic effect of insufficient energy production and the potential dysregulation of factors, such as Rab GTPases, which are integral for membrane trafficking (Hutagalung & Novick, 2011). Although we could detect a few Ronin ko cells even later, at E7.5, their small contribution was not enough to indicate whether these cells preferentially reside in a certain region (anterior/posterior) of the epiblast. In addition to the proliferation defect, it is possible that the donor Ronin ko cells are outcompeted by the cells of the host embryo, as a recent study showed that the so-called loser cells, which exhibit mitochondrial dysfunction, are eliminated in the post-implantation epiblast (preprint: Lima *et al*, 2020).

Although we could not fully examine the developmental capacity of Ronin ko ESC in the post-implantation embryo, these cells exhibited a limited potential for early lineage differentiation *in vitro*. A previous analysis using a Ronin-lacZ reporter showed a

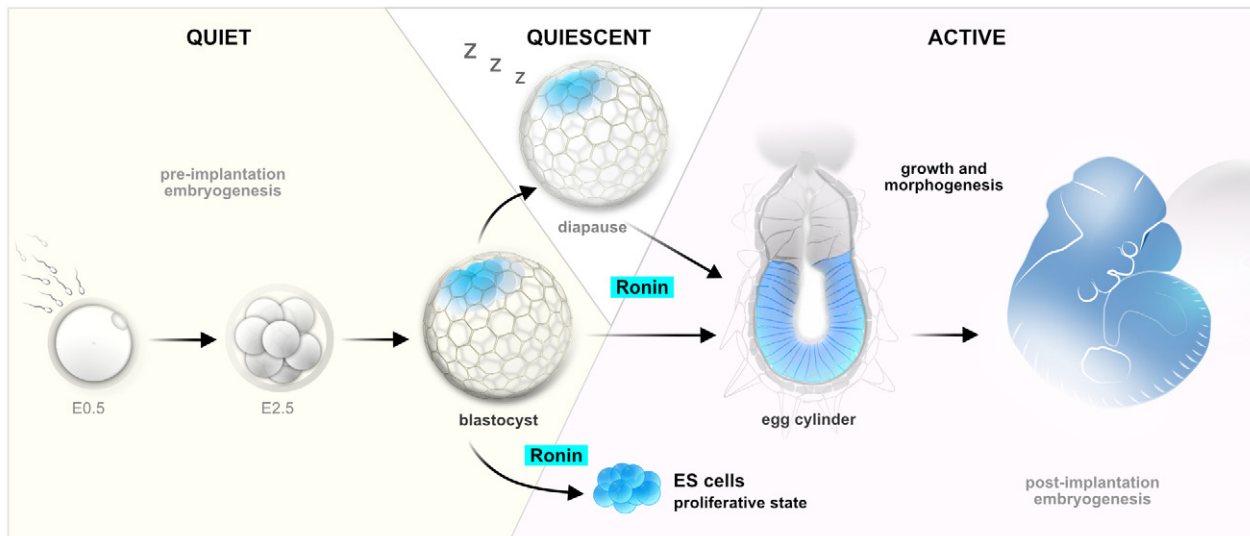


Figure 8. Ronin function during pre- to post-implantation transition and establishment of ESC lines.

Ronin is dispensable for the development of the pluripotent lineage during the “quiet” pre-implantation embryogenesis, but it is critical for exit of embryo dormancy and for providing enough metabolic capacity for the post-implantation epiblast to support cell proliferation and morphogenesis.

complex expression pattern in the developing conceptus: Ronin expression was found in the cardiac crescent at E7.5–E8.25 and in the heart, thalamus, branchial arched and posterior neuropore at E9.5. Ronin depletion in the embryonic heart resulted in a decrease of proliferating cells without significant activation of apoptosis (Fujita *et al*, 2017). Similarly, Ronin function was required for proliferation of the retinal progenitor cells (RPC). In both the RPC and the developing heart, Ronin binds and regulates genes associated with energy metabolism and biosynthesis (Poche *et al*, 2016; Fujita *et al*, 2017). The critical targets of Ronin in the RPC are ETC complexes I, III and IV, and loss of Ronin in these cells resulted in G1- to S-phase arrest and excessive neurogenic differentiation (Poche *et al*, 2016). In contrast, Ronin ko ESC in our study exhibited slow progression through the cell cycle, without preferential accumulation in a particular phase. Moreover, the establishment of a quiescent state in Ronin ko ESC promoted the expression of naïve pluripotency genes and tuned down the expression of primed markers. In the light of these observations, it would be interesting to determine whether Ronin expression is silenced in slowly cycling/quiescent adult stem cells and potentially upregulated in transiently amplifying progenitors. This would point to a common principle, in which slow progression through the cell cycle increases a cell’s responsiveness to the signalling that maintains the stem cell state and, at the same time, buffers the influence of internal and external pro-differentiation cues.

Materials and Methods

Mice and embryos

Animal experiments and husbandry were performed according to the German Animal Welfare guidelines and approved by the

Landesamt für Natur, Umwelt und Verbraucherschutz Nordrhein-Westfalen (State Agency for Nature, Environment and Consumer Protection of North Rhine-Westphalia). The mice used in this study were at the age from 6 weeks to 5 months. The animals were maintained under a 14-h light/10-h dark cycle with free access to food and water. Female mice were housed in groups of up to 4 per cage, and male stud mice were housed individually. Embryos for experiments were obtained from wild-type B6C3F1 and CD1 strains. E2.5 embryos were collected in M2 medium (Sigma), and after removal of Zona pellucida via Tyrode’s solution (Sigma), the morulae were aggregated with fluorescently labelled ESC. The chimeric embryos were cultured in KSOM medium (Millipore) and then analysed or transferred into pseudopregnant females. Diapause was induced via ovariectomy. The pregnancy during diapause was maintained by a daily injection of 3 mg medroxyprogesterone 17-acetate. Reactivation of embryos was induced by injection of 25 ng β -estradiol.

Cell lines

ESC were maintained on mitotically inactivated DR-4 feeders in DMEM medium supplemented with 15% FBS, 2 mM L-glutamine, 1 mM sodium pyruvate, 0.1 mM non-essential amino acids, 50U/ml penicillin-streptomycin, 0.1 mM 2-mercaptoethanol and 4 ng/ml Lif (prepared in house) at 37°C and 5% CO₂ atmosphere in air. Cre/loxP recombination in Ronin fl/del Cre-ERT2 ESC was induced using 500 nM 4OHT. The Ronin-FLAG transgene was cloned into the pIB12-PB-hCMV1-cHA-IRES-Venus plasmid, which contains tetracycline response elements and co-transfected with transposase (pIB1-PyCAG-PBase) and tetracycline-controlled transactivator (pIB11-PB-CAG-rtTAM2-IRES-Neo) plasmids, followed by selection with G418 (300 μ g/ml). Tet-on transgene expression of ecto-Ronin was stimulated using 1 μ g/ml of Dox.

3D cell culture

Ronin fl/del or day 4 Ronin del/del ESC were dissociated using 0.05% Trypsin-EDTA, pelleted by centrifugation (5 min/1,000 rpm), then washed with PBS and re-pelleted. After that, the cells were resuspended in Matrigel (Corning, 356231; 2,000 cells per 1 μ l of Matrigel), and 20 μ l of the cell suspension was plated per single well of an 8-well ibidi μ -plate. To solidify the hydrogel, the plate was incubated for 2–3 min at 37°C. The wells were filled with N2B27 medium supplemented with 12 ng/ml Fgf2, 20 ng/ml Activin A and 1% KSR, and the cells were cultured for 48 h at 37°C and 5% CO₂ atmosphere in air.

Western blot

The cells were lysed using buffer containing 10 mM Tris-HCl pH 7.6, 150 mM NaCl, 2 mM MgCl₂, 2 mM EDTA, 0.1% Triton X-100, 10% Glycerol and 1 \times protease inhibitor cocktail (cOmplete ULTRA). The lysate was incubated for 20 min on ice, and the protein concentration was determined using the BCA assay. The proteins were loaded into PAA gel and transferred to PVDF membrane followed by blocking in 5% dry milk in PBST for 30 min. The membrane was incubated with primary antibodies at 4°C, overnight. On the next day, the membrane was washed with PBST and incubated with secondary antibodies conjugated to HRP for 2 h. The proteins were detected using ECL Plus and exposed to autoradiography films.

Immunofluorescence

Cells or embryos were fixed with 4% PFA and then permeabilised with 0.3% Triton for 10 min. Primary antibodies were applied in blocking buffer of 2% FCS in PBS for 24 h at 4°C. On the next day, the samples were washed using 1% FCS in PBS and incubated in secondary antibody solution for another 24 h at 4°C. ESC were directly imaged in the ibidi μ -plates, whereas embryos were mounted on glass-bottom plates, in drops of 1% FCS/PBS under mineral oil. Primary antibodies and dilutions: Mouse anti-Ronin (BD Pharmingen, 562548, 1:200), Mouse anti-Nanog (Cell signaling technology, 8822, 1:300), Goat anti-Sox17 (R&D systems, AF1924, 1:300), Mouse anti-Oct4 (Cell signalling technology, 83932, 1:300), Mouse anti-Pard6B1 (Santa Cruz Biotechnology, sc-166405, 1:300), Rabbit monoclonal anti-Sox2 (Cell signalling technology, 23064, 1:300), Mouse anti-E-Cadherin (BD Biosciences, 610182, 1:300), Rat anti-Podocalyxin (R&D systems, MAB1556, 1:300), Rabbit anti-RFP (Rockland Immunochemicals, Inc. 600-401-379, 1:200), Rabbit anti-Gata6 (Cell Signaling Technology, 5851, 1:200), Rabbit anti-Vimentin (Cell Signaling Technology, 5741, 1:200). Secondary antibodies and dilutions: Alexa 594 donkey Anti-Rabbit IgG (H + L) (1:200), Alexa 488 donkey Anti-Rabbit IgG (H + L) (1:200), Alexa 488 donkey Anti-Mouse IgG (H + L) (1:200), Alexa 647 donkey Anti-Rat IgG (H + L) (1:200), Alexa 647 donkey Anti-mouse IgG (H + L) (1:200), Alexa 647 donkey Anti-Goat IgG (H + L) (1:200), Alexa 488 donkey Anti-Rabbit IgG (H + L) (1:200). F-actin was stained using Alexa Fluor 647 Phalloidin. Images were acquired using Leica SP5, Leica SP8 and Zeiss LSM780 confocal microscopes and analysed using Fiji and Imaris software.

Generation of teratomas and immunohistochemistry

Scid mice were injected subcutaneously with a 100 μ l suspension containing 5 million ESC in PBS. Solid tumours were isolated and fixed at 4°C overnight in 4% PFA/PBS. The samples were dehydrated in an ethanol series (30%, 50%, 70% and 100% in PBS) for 2 h each, followed by two 10-min incubations in 100% xylene, and then transferred to paraffin. Samples embedded into paraffin blocks were sectioned at 7 μ m using an HM355S microtome (Thermo). Haematoxylin/eosin staining was carried out as described previously (Stemmler & Bedzhov, 2010).

In vitro differentiation of ESC

The *in vitro* differentiation of ESC using the EB assay was carried out as previously described (Bedzhov *et al*, 2013). Briefly, ESC were trypsinised and suspended in DMEM medium supplemented with 20% FCS, 10 U/ml Pen/Strep and 0.15 mM β -mercaptoethanol. Drops of 30 μ l suspension, containing approximately 300 cells, were placed on the under-surface of a lid, and simple EBs were formed after 2 days of culture. The simple EBs were then transferred into non-adhesive plates and cultured in suspension for 3 days. After that, the EBs were transferred in tissue culture plates, where they attached and the cells spread out during the next 7 days.

Fluorescence-activated cell sorting (FACS)

Cells were dissociated using trypsin and transferred into PBS supplemented with 3% FCS. FACSaria IIu sorter (BD biosciences) was used for sorting and analysis. Cell cycle analysis using EdU assay (Thermo) and cell death analysis using Annexin V assay (Thermo) were performed according to the manufacturer's instructions. Flowjo software (TreeStar) was used for data analysis.

OP-puro assay

The OP-puro assay (Abcam, ab239725) was carried out following the manufacturer's instructions.

TMRE assay

The cells were stained with 400 nM MitoTracker Green FM (Thermo) for 30 min and then washed two times with PBS and one time with ESC culture medium. After that, the cells were stained with 14 nM TMRE (AAT Bioquest) for 30 min, washed once with PBS and trypsinised. The cell pellet was resuspended in FACS buffer (3% FCS in PBS) prior to FACS analysis for MitoTracker Green FM and TMRE signal.

Mitochondrial stress test assay

The OCR of Ronin fl/del and Ronin del/del ESC was measured with the Seahorse XFe96 Extracellular Flux Analyzer. The cells were seeded on gelatine-coated 96-well XF cell culture microplates 24 h prior to analysis. Fresh medium was supplied before starting the OCR analysis. The assay was carried out according to the manufacturer's instructions using 0.5 μ M Oligomycin, 1 μ M FCCP and 0.5 μ M Rotenone/Antimycin A. After the OCR measurement, the

cell number per well was determined by labelling the nuclei with 2 µg/ml Hoechst 33342.

Electron microscopy

The samples (ESC and embryos) were initially fixed with 2% PFA, 2% glutaraldehyde in 0.1 M cacodylate buffer, pH 7.4. After that, specimens were post-fixed in 1% osmium tetroxide, 1.5% potassium ferrocyanide in 0.1 M cacodylate buffer, followed by stepwise dehydration in ethanol, including 0.5% uranyl acetate en bloc staining in 70% ethanol. Final dehydration was performed in propylene oxide, and samples were further embedded in epon. Ultrathin sections of 60 nm were cut using ultramicrotome (UC6, Leica), collected on copper grids, counterstained with lead and examined on a Tecnai-12 transmission electron microscope at 80 kV (Thermo Fisher Scientific). Representative areas were imaged on a 2K CCD camera (Veleta, EMSIS).

RNA-seq analysis

Transcript expression from RNA-seq was quantified using Salmon (version 1.2.1) with parameters "--seqBias" using a transcriptome index created from *Mus musculus* genome version GRCm38 (Ensembl release 99). Transcript quantifications were imported into R and associated with genes using the tximport package (version 1.14.2). Differential expression analysis was performed using DESeq2 (version 1.26.0). Genes were considered significantly differentially expressed between two conditions if the comparison had an adjusted *P*-value < 0.05.

The variance stabilising transformation was applied to data for the purposes of visualisation using PCA or heatmaps. PCA was performed using the "prcomp" R function on the top 500 most variable genes across all samples. For gene expression clustering, we considered genes that were significantly differentially expressed in at least one comparison. Gene expression matrices were transformed to row Z-scores and clustered using k-means clustering using the "kmeans" R function. The appropriate number of clusters was assessed using the elbow method.

Gene Ontology enrichment analysis was carried out using the "compareCluster" or "enrichGO" function from the clusterProfiler package (version 3.14.3) with a *q*-value threshold of 0.1. Results were simplified to remove highly similar GO terms based on semantic similarity using the "simplify" function with the Wang method and a similarity threshold of 0.7 (GOSemSim version 2.12.1).

Gene set enrichment analysis was performed using the fgsea package (version 1.12.0) on the Hallmark and Biocarta gene sets from MSigDB (version 7.1), with genes ranked by the test statistic from DESeq2.

RNA-seq data analysis and visualisation were carried out using R (version 3.6.3). The ggplot2 (version 3.3.2) and ComplexHeatmap (version 2.2.0) R packages were used for data visualisation, and the dplyr (version 1.0.1) and purrr (version 0.3.4) packages were used for general data analysis.

ChIP-seq analysis

ChIP-seq data were obtained from SRR1014799 (Hnisz et al, 2013) and mapped to the GRCm38 genome using Bowtie2 (version 2.4.1).

Mapped reads were filtered to remove alignments with quality scores less than 30 as well as secondary and supplementary alignments. PCR duplicates were marked using sambamba (version 0.6.8). Coverage tracks were generated using the bamCoverage tool from deepTools (version 3.4.3) with the following parameters: "--of bigwig --binSize 10 --normalizeUsing CPM --extendReads 200 --ignoreDuplicates --minMappingQuality 30". ChIP-seq peaks were called using MACS2 (version 2.2.7.1) with default parameters. Promoter ChIP-seq signal was calculated using a 1-kb window around the annotated transcription start site. For genes with multiple annotated transcription start sites, the one with highest ChIP-seq coverage was retained. ChIP-seq coverage values above the 99th percentile were replaced with the 99th percentile, and then, all coverage values were rescaled to lie between 0 and 1.

Data availability

Further information and requests for resources and reagents should be directed to the corresponding author Ivan Bedzhov (ivan.bedzhov@mpi-muenster.mpg.de). The RNA-seq datasets are available from the ArrayExpress repository. ArrayExpress accession: E-MTAB-10024 (<http://www.ebi.ac.uk/arrayexpress/experiments/E-MTAB-10024/>).

Expanded View for this article is available online.

Acknowledgements

We thank Prof. Dr. Ralf H. Adams and Prof. Dr. Dietmar Vestweber for providing access to key infrastructure, equipment and reagents; Dr. Anika Witten for the RNA-sequencing and Dr. Celeste Brenneka for proofreading the manuscript. This work was supported by the German Research Foundation (DFG) Emmy Noether grant (BE 5800/1-1) and Collaborative Research Center 1348 "Dynamic Cellular Interfaces" grant (1348/1, B09) to I.B. Open Access funding enabled and organized by Projekt DEAL.

Author contributions

IB, KS and TGT conceived the study, designed experiments and interpreted the results; IB and KS: wrote the manuscript; EIS and JMV performed the bioinformatics analysis; BD, KS, KB and BR performed the TMRE and Seahorse assays; RF performed the Annexin V assay; TGT, RC and NG analysed Ronin expression in early embryos; BD, KS and TGT performed teratoma, embryoid body and marker expression analysis; HB and TGT generated the ecto-Ronin cells and characterised the ESC proliferation rate; LK and NKR generated ESC/embryo chimeras and performed embryo transfers; DZ and KM performed the transmission electron microscopy; MS performed FACS analysis; HRS contributed to the conception and discussion of the project and provided reagents, materials and access to equipment; TPZ and MD generated Ronin conditional ko ESC line.

Conflict of interest

The authors declare that they have no conflict of interest.

References

- Bedzhov I, Alotaibi H, Basilicata MF, Ahlborn K, Liszewska E, Brabletz T, Stemmler MP (2013) Adhesion, but not a specific cadherin code, is indispensable for ES cell and induced pluripotency. *Stem Cell Res* 11: 1250–1263

- Bedzhov I, Zernicka-Goetz M (2014) Self-organizing properties of mouse pluripotent cells initiate morphogenesis upon implantation. *Cell* 156: 1032–1044
- Boroviak T, Loos R, Lombard P, Okahara J, Behr R, Sasaki E, Nichols J, Smith A, Bertone P (2015) Lineage-specific profiling delineates the emergence and progression of naive pluripotency in mammalian embryogenesis. *Dev Cell* 35: 366–382
- Chen Xi, Xu H, Yuan P, Fang F, Huss M, Vega VB, Wong E, Orlov YL, Zhang W, Jiang J et al (2008) Integration of external signaling pathways with the core transcriptional network in embryonic stem cells. *Cell* 133: 1106–1117
- Cree LM, Samuels DC, de Sousa Lopes SC, Rajasimha HK, Wonnapijit P, Mann JR, Dahl HH, Chinnery PF (2008) A reduction of mitochondrial DNA molecules during embryogenesis explains the rapid segregation of genotypes. *Nat Genet* 40: 249–254
- Crowley LC, Christensen ME, Waterhouse NJ (2016) Measuring mitochondrial transmembrane potential by TMRE staining. *Cold Spring Harb Protoc* 2016: pdb.prot087361
- Dejosez M, Krumenacker JS, Zitur LJ, Passeri M, Chu LF, Songyang Z, Thomson JA, Zwaka TP (2008) Ronin is essential for embryogenesis and the pluripotency of mouse embryonic stem cells. *Cell* 133: 1162–1174
- Dejosez M, Levine SS, Frampton GM, Whyte WA, Stratton SA, Barton MC, Gunaratne PH, Young RA, Zwaka TP (2010) Ronin/Hcf-1 binds to a hyperconserved enhancer element and regulates genes involved in the growth of embryonic stem cells. *Genes Dev* 24: 1479–1484
- Dejosez M, Zwaka TP (2012) Pluripotency and nuclear reprogramming. *Annu Rev Biochem* 81: 737–765
- Fan R, Kim YS, Wu J, Chen R, Zeuschner D, Mildner K, Adachi K, Wu G, Galatidou S, Li J et al (2020) Wnt/Beta-catenin/Esrrb signalling controls the tissue-scale reorganization and maintenance of the pluripotent lineage during murine embryonic diapause. *Nat Commun* 11: 5499
- Fenelon JC, Banerjee A, Murphy BD (2014) Embryonic diapause: development on hold. *Int J Dev Biol* 58: 163–174
- Fu Z, Wang B, Wang S, Wu W, Wang Q, Chen Y, Kong S, Lu J, Tang Z, Ran H et al (2014) Integral proteomic analysis of blastocysts reveals key molecular machinery governing embryonic diapause and reactivation for implantation in mice. *Biol Reprod* 90: 52
- Fujita J, Freire P, Coarfa C, Benham AL, Gunaratne P, Schneider MD, Dejosez M, Zwaka TP (2017) Ronin governs early heart development by controlling core gene expression programs. *Cell Rep* 21: 1562–1573
- Govindasamy N, Duethorn B, Oezgueldez HO, Kim YS, Bedzhov I (2019) Test-tube embryos - mouse and human development *in vitro* to blastocyst stage and beyond. *Int J Dev Biol* 63: 203–215
- Hackett JA, Surani MA (2014) Regulatory principles of pluripotency: from the ground state up. *Cell Stem Cell* 15: 416–430
- Hnisz D, Abraham BJ, Lee TI, Lau A, Saint-Andre V, Sigova AA, Hoke HA, Young RA (2013) Super-enhancers in the control of cell identity and disease. *Cell* 155: 934–947
- Houghton FD (2006) Energy metabolism of the inner cell mass and trophectoderm of the mouse blastocyst. *Differentiation* 74: 11–18
- Hutagalung AH, Novick PJ (2011) Role of Rab GTPases in membrane traffic and cell physiology. *Physiol Rev* 91: 119–149
- Leese HJ (2012) Metabolism of the preimplantation embryo: 40 years on. *Reproduction* 143: 417–427
- Lima A, Burgstaller J, Sanchez-Nieto JM, Rodriguez TA (2018) The mitochondria and the regulation of cell fitness during early mammalian development. *Curr Top Dev Biol* 128: 339–363
- Lima A, Lubatti G, Burgstaller J, Hu D, Green A, Gregorio AD, Zawadzki T, Pernaute B, Mahmammodov E, Dore M et al (2020) Differences in mitochondrial activity trigger cell competition during early mouse development. *bioRxiv* <https://doi.org/10.1101/2020.01.15.900613> [PREPRINT]
- Liu J, Xu Y, Stoleru D, Salic A (2012) Imaging protein synthesis in cells and tissues with an alkyne analog of puromycin. *Proc Natl Acad Sci U S A* 109: 413–418
- Martello G, Bertone P, Smith A (2013) Identification of the missing pluripotency mediator downstream of leukaemia inhibitory factor. *EMBO J* 32: 2561–2574
- Mishra P, Chan DC (2014) Mitochondrial dynamics and inheritance during cell division, development and disease. *Nat Rev Mol Cell Biol* 15: 634–646
- Mitchell P (1961) Coupling of phosphorylation to electron and hydrogen transfer by a chemi-osmotic type of mechanism. *Nature* 191: 144–148
- Poché RA, Zhang M, Rueda EM, Tong X, McElwee ML, Wong L, Hsu C-W, Dejosez M, Burns AR, Fox DA et al (2016) RONIN is an essential transcriptional regulator of genes required for mitochondrial function in the developing retina. *Cell Rep* 14: 1684–1697
- Quinn P, Wales RG (1971) Adenosine triphosphate content of preimplantation mouse embryos. *J Reprod Fertil* 25: 133–135
- Rival T, Macchi M, Arnaune-Pelloquin L, Poidevin M, Maillet F, Richard F, Fatmi A, Belenguer P, Royet J (2011) Inner-membrane proteins PMI/TMEM11 regulate mitochondrial morphogenesis independently of the DRP1/MFN fission/fusion pathways. *Embo Rep* 12: 223–230
- Seifert BA, Dejosez M, Zwaka TP (2017) Ronin influences the DNA damage response in pluripotent stem cells. *Stem Cell Res* 23: 98–104
- Shi YU, Zhou W, Cheng L, Chen C, Huang Z, Fang X, Wu Q, He Z, Xu S, Lathia JD et al (2017) Tetraspanin CD9 stabilizes gp130 by preventing its ubiquitin-dependent lysosomal degradation to promote STAT3 activation in glioma stem cells. *Cell Death Differ* 24: 167–180
- Snow MHL (1977) Gastrulation in the mouse: growth and regionalization of the epiblast. *Development* 42: 293–303
- Stemmler MP, Bedzhov I (2010) A Cdh1HA knock-in allele rescues the Cdh1^{-/-} phenotype but shows essential Cdh1 function during placentalation. *Dev Dyn* 239: 2330–2344
- Tamai S, Iida H, Yokota S, Sayano T, Kiguchiya S, Ishihara N, Hayashi JI, Mihara K, Oka T (2008) Characterization of the mitochondrial protein LETM1, which maintains the mitochondrial tubular shapes and interacts with the AAA-ATPase BCS1L. *J Cell Sci* 121: 2588–2600
- Ye S, Li P, Tong C, Ying QL (2013) Embryonic stem cell self-renewal pathways converge on the transcription factor Tfcp2l1. *EMBO J* 32: 2548–2560
- Yoon W, Hwang SH, Lee SH, Chung J (2019) Drosophila ADCK1 is critical for maintaining mitochondrial structures and functions in the muscle. *PLoS Genet* 15: e1008184
- Zhang J, Zhao J, Dahan P, Lu V, Zhang C, Li H, Teitel MA (2018) Metabolism in pluripotent stem cells and early mammalian development. *Cell Metab* 27: 332–338
- Zwaka TP (2008) Ronin and caspases in embryonic stem cells: a new perspective on regulation of the pluripotent state. *Cold Spring Harb Symp Quant Biol* 73: 163–169



License: This is an open access article under the terms of the Creative Commons Attribution-NonCommercial-NoDerivatives License, which permits use and distribution in any medium, provided the original work is properly cited, the use is non-commercial and no modifications or adaptations are made.